energies

MDPI

Article

Sky Luminance Distribution Models: A Comparison with Measurements from a Maritime Desert Region

Khalid Alshaibani [1,*], Danny Li [2] and Emmanuel Aghimien [2]

[1] College of Architecture and Planning, Imam Abdulrahman Bin Faisal University, Dammam 34212, Saudi Arabia

[2] Building Energy Research Group, Department of Architecture and Civil Engineering, City University of Hong Kong, Tat Chee Avenue, Kowloon, Hong Kong, China; bcdanny@cityu.edu.hk (D.L.); eaghimien2-c@my.cityu.edu.hk (E.A.)

* Correspondence: kshaibani@iau.edu.sa

Received: 11 September 2020; Accepted: 16 October 2020; Published: 19 October 2020

Abstract: The effective use of daylight is a function of the luminance of the sky exposed to the glazing system. Therefore, accurate data about the luminance distribution of the sky are necessary for the optimum use of daylight. This paper compares seven models for estimating the angular sky luminance distribution. They were selected based on the ability to be used with all sky conditions and to determine the luminance of the sky from solar radiation. Measurements of solar radiation, sky luminance, and sky radiance were taken in a "maritime desert region" in Saudi Arabia. The results showed that the "Perez 93" model performed better than the other models tested, but there is a need for more studies to identify more accurate models for use in similar climatic conditions.

Keywords: sky luminance; daylighting; maritime desert region

1. Introduction

The use of daylight in buildings can be attributed to different conditions and varying design criteria. One major benefit of using daylight is that it reduces energy consumption [1–3]. Other design criteria related to the use of daylight in buildings are its physiological and psychological impact on people and the satisfaction of the occupant [4–8]. These valuable effects make daylight an aesthetic tool for the architect and a qualitative asset for the users of a building. The effective use of daylight is mainly a function of the luminance of the sky exposed to the glazing system. Therefore, accurate data about the luminance distribution of the sky are needed for the use of daylight.

In 2003, in order to help make better use of daylight, the International Commission on Illumination (CIE) proposed a general sky model [9,10] which is now known as the "ISO/CIE Standard General Skies" [11]. This standard defines the sky luminance distribution into conditions that range from overcast to clear sky. Several methods have been proposed in order to fit a sky into one (or more) of theses 15 sky types [12–16]. However, to fit a sky into one of the CIE skies, measurements of luminance are needed. Such data are not available in many regions of the world, so sky models that estimate the luminance distribution of the sky from measurements of the available solar radiation seem to be a very helpful option. Several sky luminance models that are based on insolation condition have been proposed. However, the accuracy of these models varies because of the assumptions they use and the differences in climatic conditions from one site to another [15,17–23]. These sky models have been used in computer programs, in which daylight simulation can be used to evaluate the daylight performance of a proposed or existing building for any period of time. Such evaluation can be based on several criteria. These include visual comfort [24–27], energy performance [25,27], and adequacy of

internal lighting conditions [28,29]. However, different sky models can lead to different quantitative and qualitative results [30–32].

The aim of this paper is to evaluate some of these sky models using luminance and solar radiation measurements taken in a maritime desert region in Saudi Arabia.

2. All Sky Luminance Distribution Models

For this study, seven sky luminance distribution models were selected. These models have been investigated in previous studies under different climatic conditions [21,23,33–35]. The reason for selecting these models is that they can estimate the luminance distribution for any sky conditions based on available solar radiation data. Descriptions of the models are presented in the following sections.

2.1. Perraudeau Model

One of the earliest models that relates sky luminance to solar radiations was proposed by Perraudeau in 1988 [36]. This model calculates the sky luminance based on the diffuse horizontal irradiance. The luminance of a sky element is a product of three functions, depending on the angular distance to the sun, the angle between the zenith and the sky point, and the zenith angle of the sun (Figure 1):

$$Lv = Eed\ f'(\chi)\ g'(Z)\ h'(Zs) \tag{1}$$

where

$$f'(\chi) = a_1 + b_1 \exp(-3\chi) + c_1 \cos^2 \chi \tag{2}$$

$$g'(Z) = a_2 + b_2 (\cos Z)^{0.6} \tag{3}$$

$$h'(Zs) = a_3 + b_3 \cos Zs + c_3 \sin Zs \tag{4}$$

where ai, bi, and ci are adjustable coefficients for each of the five sky conditions (overcast to clear) proposed by this model and defined by a cloud index, which is a normalized cloud ratio.

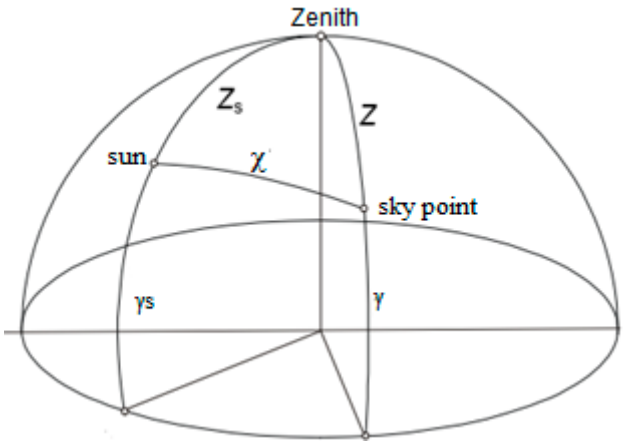

Figure 1. Angles that define the position of the sun and a sky point.

2.2. Brunger Model

The Brunger model estimates radiance rather than luminance [37]. However, luminance and radiance have nearly identical relative distributions [38]. The luminance of a sky point (Lv) can be found from the following:

$$Lv = Eed\ [\ a_0 + a_1 \sin\gamma + a_2 \exp(-a_3 \chi)]$$

$$[\pi\ (a_0 + 2\ a_1/3) + 2\ a_2\ I\ (Zs, a_3)] \tag{5}$$

where a_0, a_1, a_2, and a_3 are the adjustable coefficients based on the ratio of global irradiance to extraterrestrial irradiance and the ratio of diffuse irradiance to global irradiance. I (Zs, a_3) is a normalizing function.

2.3. Harrison Model

Harrison proposed two equations for estimating the luminance distribution of overcast sky (Lvo) and clear sky (Lvc) [39]. Based on opaque cloud cover, the luminance of a sky element (Lv) can be found through a linear combination of the two equations:

$$Lv = C\ Lo + (1 - C)\ Lvc \tag{6}$$

where

$$Lo = 0.4 + 0.21\ Zs + 0.27 \cos Z + 1.45 \exp(-2.14\ \chi)$$

$$Lvc = [1.28 + 147 \exp(-11.1\chi) + 4.58 \cos 2\ \chi \cos Zs] \tag{7}$$

$$[1 - \exp(-0.42/\cos Z)]\ [1 - \exp(-0.67/\cos Zs)] \tag{8}$$

In this study, the ratio of horizontal sky irradiance to global horizontal irradiance (C) is used instead opaque of cloud cover [22].

2.4. Matsuura Model

This model uses the CIE standard sky types; clear, intermediate, and overcast [40]. The governing parameter in this model is the ratio of horizontal sky illuminance to the global horizontal illuminance. In this study, the ratio of horizontal sky irradiance to global horizontal irradiance is used instead:

$$Lv = a_{cl}\ L_{cie\_cl} + a_{in}\ L_{cie\_in} + a_{ov}\ L_{\ cie\_ov} \tag{9}$$

where

$L_{cie\text{-}cl}$ is sky luminance from the CIE clear sky model [41];

$$L_{cie\_cl}/Lz = f(\chi)\ \varphi(Z)/f(Zs)\ \varphi(90^\circ) \tag{10}$$

$$f\ (\chi) = 1 + c\ \{\exp(d\ \chi) - \exp(d\ \pi)\} + e \cos 2\ \chi) \tag{11}$$

$$\varphi(\gamma) = 1 + a \exp(b/\sin\gamma) \tag{12}$$

$L_{cie\text{-}ov}$ is sky luminance from the CIE overcast sky model [42];

$L_{cie\text{-}in}$ is sky luminance from Nakamura's sky model [43].

The adjustable coefficients (a_{cl}, a_{in}, and a_{ov}) are based on three ranges of illuminance cloud ratio (diffuse horizontal sky illuminance to global illuminance).

2.5. ASRC-CIE Model (Pereze90)

This model uses the same approach used in the Matsuura model. However, in this model, four CIE sky models and three ranges of sky conditions are used [22,44]. The CIE skies are the clear sky [41], the intermediate sky [43], the overcast sky [42], and the high turbidity clear sky models [43]. The ratio of the luminance of an arbitrary sky element to the zenith luminance, is given by:

$$Lv = Lz\ (b_{cl}\ L_{cie\_cl} + b_{ct}\ L_{cie\_ct} + bi\ L_{cie\_in} + b_{ov}\ L_{cie\_ov}) \tag{13}$$

Sky condition is based on a clearness index (ε) and sky brightness index (Δ) which is used to decide on the contribution from each of the four CIE sky models through the adjustable coefficients (b_{cl}, b_{ct}, b_i, and b_{ov}):

$$\varepsilon = \frac{\frac{Eed+Ees}{Eed} + 1.041\ Zs^3}{1 + 1.041\ Zs^3} \quad (14)$$

$$\Delta = m\ \frac{Eed}{Eeo} \quad (15)$$

The luminance at the zenith can be assumed with any value. This is because this study will evaluate the relative distribution rather than dealing with absolute values.

2.6. Perez Model (Perez 93)

The CIE clear sky [41] is used in this model [45]. It is based on five adjustable coefficients which account for luminance distributions ranging from totally overcast to very clear:

(a) Darkening or brightening at the horizon.
(b) Luminance gradient near the horizon.
(c) Relative intensity of the circumsolar region.
(d) Width of the circumsolar region.
(e) The relative backscattered light.

The values of these coefficients are chosen as a function of sky condition, identified by the values of Perez's clearness index (ε) and the sky brightness index (Δ) used [44].

$$Lv/Lz = f(\chi)\ \varphi(Z)/f(Zs)\ \varphi(0^\circ) \quad (16)$$

$$f\ (\chi) = 1 + c\ \{\exp\ (d\ \chi) - \exp\ (d\ \pi)\} + e\ \cos 2\ \chi) \quad (17)$$

$$\varphi(\gamma) = 1 + a\ \exp\ (b/\sin\ \gamma) \quad (18)$$

2.7. Igawa Model

Igawa proposed what he called the improved All-Sky model (i-As) [46]. Like Perez, he used the same the CIE clear sky model [41]. However, Igawa proposes a different approach for estimating the five coefficients of the model (a, b, c, d, and e) that are a function of "Cloudless index" and "Clear sky index".

3. Luminance and Solar Radiation Measurements

Data were collected for this study at a measuring station located on the roof of the College of Architecture and Planning, Imam Abdulrahman Bin Faisal University in Dammam (26°30′ N, 50°09′ E) (Figure 2). Dammam is located on the east coast of Saudi Arabia. Most of the coast is classified as a hot-dry climate zone [47]. However, because Dammam is located on the shore of the Gulf, the relative humidity is high and the area may be classified as a hot-dry maritime desert [47].

Data used in this study were collected from two sources:

1. A solar monitor station operated (Figure 2), maintained, and calibrated by King Abdullah City for Atomic and Renewable Energy [48]. The data collected from this station include: direct normal irradiance where the measurements are done with a pyrheliometer mounted in an automatic solar tracker (Solys 2—Kipp and Zonene); diffuse horizontal irradiance where the measurements are done with a shaded pyranometer (Kipp and Zonene), and global horizontal irradiance measured with an unshaded pyranometer (Kipp and Zonene).
2. A newly installed EKO sky scanner model MS 321 LR (Figure 3) was used for sky luminance measurements.

Figure 2. Solar monitoring station on the roof of the College of Architecture and Planning, Imam Abdulrahman Bin Faisal University, Dammam, Saudi Arabia.

Figure 3. The sky scanner, on the roof of the College of Architecture and Planning, Imam Abdulrahman Bin Faisal University, Dammam, Saudi Arabia.

The solar radiation measurements are based on one-minute intervals. Such raw data were tested to eliminate inaccurate measurements. This was done through the following steps [20,49]:

1. Rejecting readings of global horizontal radiation greater than 1.2 times the corresponding extraterrestrial horizontal radiation.
2. Rejecting readings of horizontal sky radiation greater than 0.8 times the corresponding extraterrestrial horizontal radiation.
3. Rejecting all readings when the solar altitude is less than five degrees.
4. Rejecting all data when the direct normal exceeds the corresponding extraterrestrial solar component.

Data from the sky scanner were obtained in 10-min intervals during daylight, from 4 April 2019 until the end of January 2020 (each scan takes up to 4.5 min). The measurements were taken at 145 different points distributed over the sky dome. The sky scanner can measure within a range of 0 to 50 Kcd/m^2. Therefore, measurements for points close to the position of the sun are affected by direct

sunlight, resulting in high readings (Figure 4). For that reason, readings above 50 are always replaced by a reading of 50 Kcd/m^2.

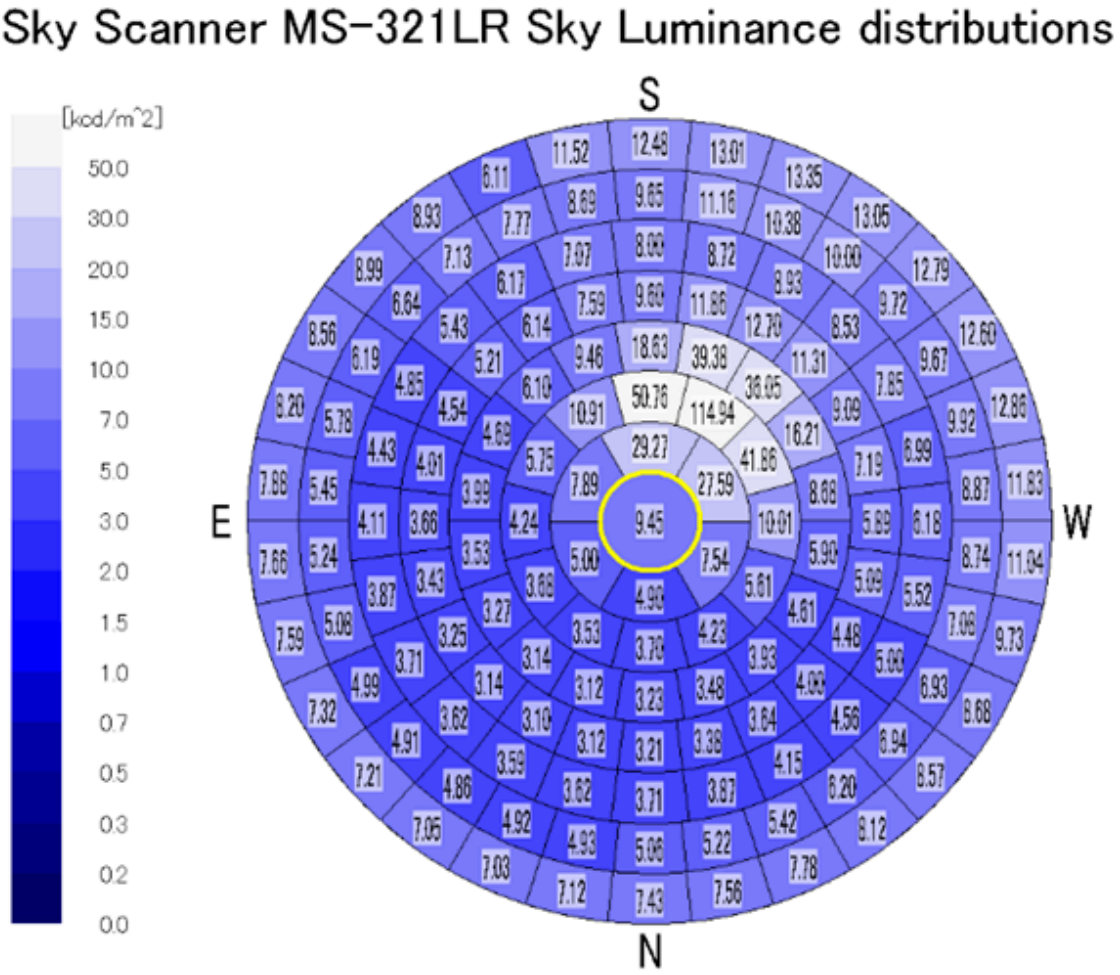

Figure 4. An example of sky luminance distribution measurements, showing the problem of high readings.

4. Results and Analysis

To evaluate the models, the luminance of a sky point was normalized to the corresponding horizontal diffuse illuminance estimated from the current scan. Sky illuminance on a horizontal surface (Ev) was estimated as follows [50,51]:

$$\mathrm{Ev} = \sum_{i=1}^{145} \mathrm{Lvi}\ \sin\ \gamma\ .\ \text{spherical area of sky element (i)} \tag{19}$$

where Lvi is the luminance of sky point i at an altitude of γ.

This approach is used because we are interested in evaluating the sky luminance distribution of the different models.

Each model was evaluated using two statistical quantities—the mean bias difference (MBD) and the root mean square difference (RMSD):

$$\mathrm{MBE} = 100\% \sum \left(\frac{\mathrm{Lpredi} - \mathrm{Lmeasi}}{\mathrm{Lmeasi}}\right)/\mathrm{N} \tag{20}$$

$$\text{RMSE} = 100\% \sum \left(\sqrt{\left(\frac{\text{Lpredi} - \text{Lmeasi}}{\text{Lmeasi}} \right)^2 / \text{N}} \right) \quad (21)$$

$$\text{Lpredi} = \text{Lpi/Edvp} \quad (22)$$

$$\text{Lmeasri} = \text{Lmi/Edvm} \quad (23)$$

The mean bias difference provides information on the long-term performance of the modeled regression equations. The root mean square difference gives information on short-term performance and it shows the scattering of data around the modeled regression equations. A high root mean square error (RMSE) indicates general inaccuracy in predicting the measured values.

RMSE and mean bias errors (MBE) were calculated for each sky model. Figure 5 summarizes all the mean bias errors (MBE) and root mean square errors (RMSE) for all scans done during the study period. The results show that four models had close results, Perez 93, Perez 90, Brunger, and Igawa. Perez 93 showed the lowest RMSE (25.5), followed by Perez 90 at 28.35, Brunger at 29.26, and Igawa at 30.52. All models overestimated sky luminance, except the Brunger model, which has a low MBE (0.93).

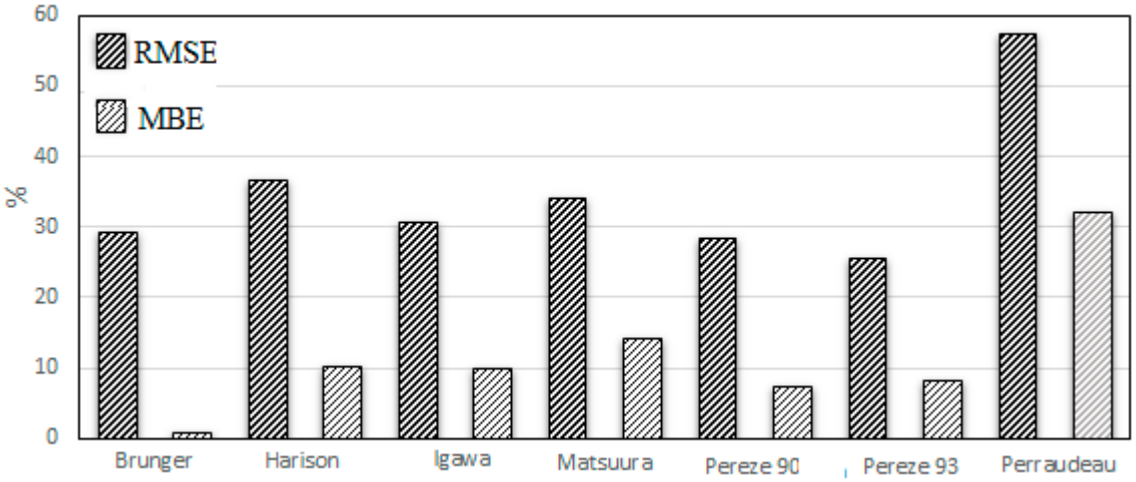

Figure 5. Root mean square errors (RMSE) and mean bias errors (MBE) for the investigated models (April 2019–January 2020).

To analyze the models according to the sky condition, results are assembled according to sky type. By using the sky ratio, which is the ratio of horizontal sky irradiance to the global horizontal irradiance [52], Dammam's sky condition for the studied period was classified. Table 1 gives the frequency of occurrence of the different sky types.

Table 1. Frequency of occurrence of the different sky types for Dammam area.

Clear (sky ratio ≤ 0.3):	22%
Partly Cloudy (0.3 < sky ratio < 0.8)	62%
Overcast (0.8 ≥ sky ratio):	16%

From Figure 6, all models produce lower RMSE for clear sky conditions compared to the RMSE for all sky conditions. Perez 93 has the lowest RMSE (22.23) for the clear sky condition. The partly cloudy sky condition accounted for about 62% of the sky condition during the studied period. MBE and RMSE values under partly cloudy conditions are similar to the results for all sky conditions (Figure 7). Again, Perez 93 has the lowest RMSE with a value of 24.38.

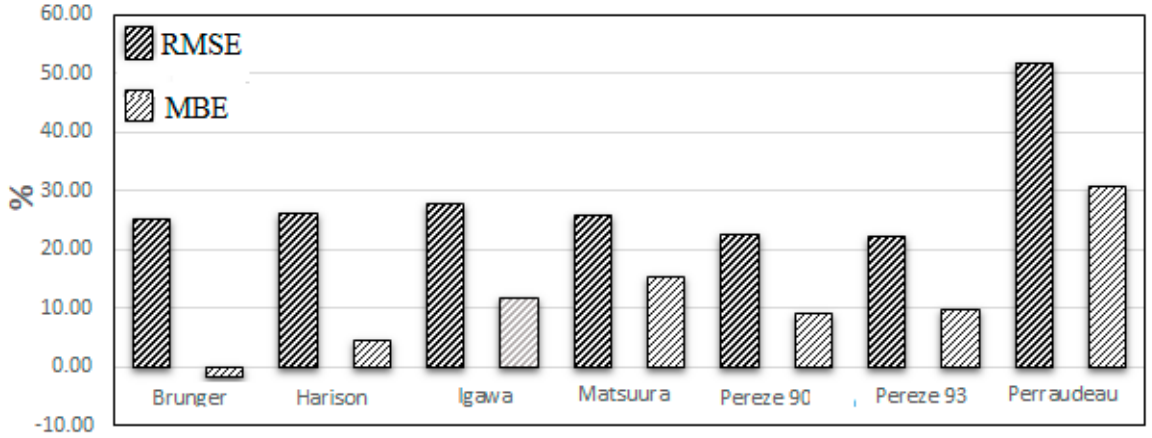

Figure 6. RMSE and MBE for the investigated models (clear sky).

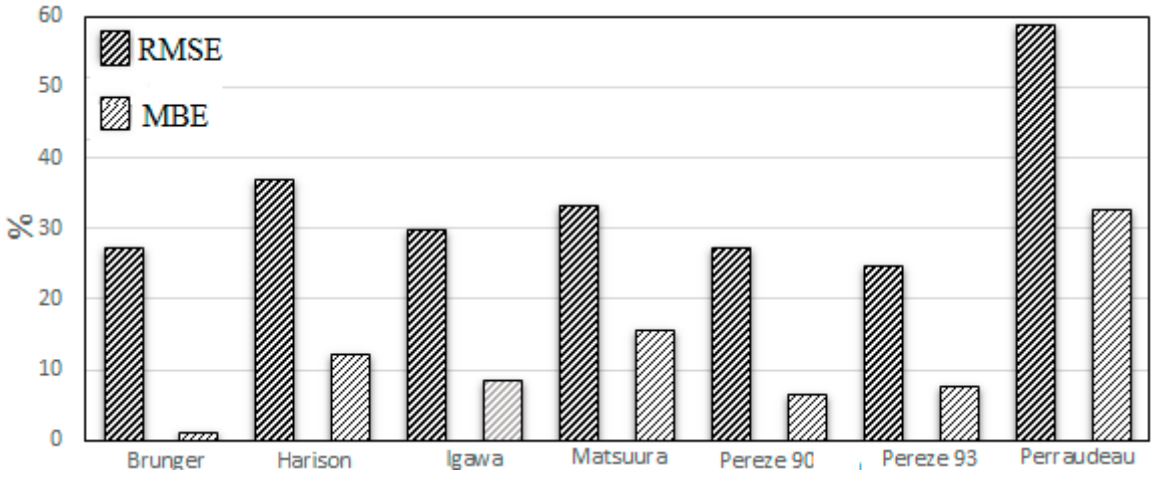

Figure 7. RMSE and MBE for the investigated models (partly cloudy sky).

For overcast sky conditions, all models show an RMSE near or above 40. The lowest RMSE value this time came from the Igawa model at 39.88 and then Perez 93 at 40.12 (Figure 8).

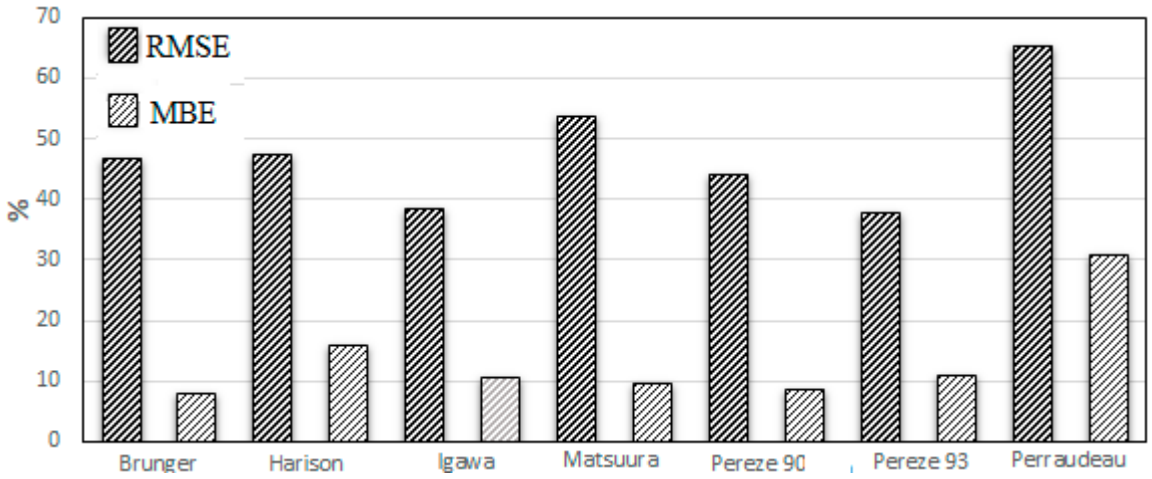

Figure 8. RMSE and MBE for the investigated models (overcast sky).

To further investigate the accuracy of the selected models, the angular distance between the sky point and the sun location (χ) was investigated. Four segments were chosen:

- Sky points within an angular distance of 45° or less from the sun.
- Sky points within an angular distance between 45° and 90° from the sun.
- Sky points within an angular distance between 90° and 135° from the sun.
- Sky points within an angular distance of more than 135° from the sun.

Figures 9 and 10 present the RSME as a function of the angular distance between the sky point and the sun (χ). Perez 93 has the lowest RMSE for $\chi < 90°$. When χ is greater than 90°, Perez 90 has the lowest RMSE, and when χ is greater than 135°, Perez 93 produces the lowest RMSE.

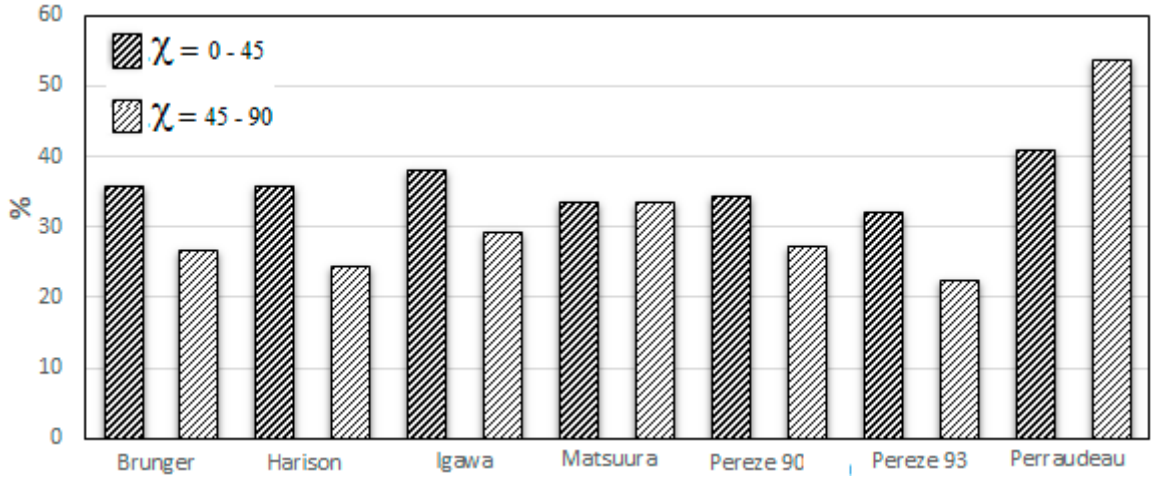

Figure 9. RMSE of the investigated models as a function of the angular distance between the sky point and sun, χ (0° to 90°).

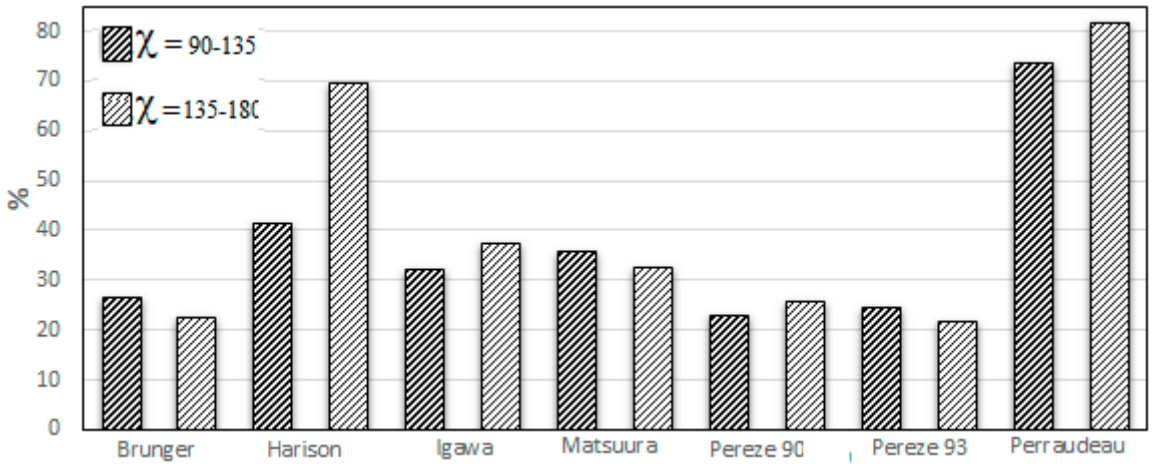

Figure 10. RMSE of the investigated models as a function of the angular distance between the sky point and sun, χ (90° to 180°).

The results showed that the Perez 93, Perez 90, Igawa, and Brunger models estimate luminance for sky points away from the sun better than when sky points are closer to the sun.

These results show that Perez 93 produces the lowest RMSE and the results for Perez 90 are nearly as low. However, the Igawa and Brunger models are other options for such climates. It is very interesting to see that the Brunger model, which was designed for radiance rather than luminance distribution, produces results similar to other models that were designed to model luminance.

5. Conclusions

This study evaluated seven sky models that can estimate sky luminance distribution through the use of horizontal sky irradiance, global horizontal irradiance, and direct normal irradiance. The study

was based on real measurements of solar radiation and luminance of the sky. These measurements were carried out in a hot-dry maritime desert region. The measurements were taken between April 2019 and January 2020. The results show the need for more study to attain more accurate sky models for similar climatic conditions. The findings illustrate that the Perez 93 model produces the best results. However, the Perez 90, Igawa, and Brunger models provide acceptable accuracy. All models perform better with clear sky conditions, while the worst results came during overcast sky conditions. In addition, Perez 93, Perez 90, Igawa, Matsuura, and Brunger perform better for sky points at an angular distance of more than 90° from the sun. It is very interesting to see that the Brunger model, which was designed for radiance rather than luminance distribution, produces results similar to other models that were designed to model luminance.

Author Contributions: Conceptualization, K.A.; methodology, K.A., D.L. and E.A.; formal analysis, K.A., D.L. and E.A.; investigation, K.A., D.L. and E.A.; writing—original draft preparation K.A.; writing—review and editing, D.L. and E.A.; visualization, K.A.; supervision, K.A.; project administration, K.A.; funding acquisition, K.A. All authors have read and agreed to the published version of the manuscript.

Funding: This research was funded by IMAM ABDULRAHMAN BIN FAISAL UNIVERSITY, grant number 2020-016-Arch.

Conflicts of Interest: The authors declare no conflict of interest.

Nomenclature

C	ratio of horizontal sky radiance to global horizontal irradiance.
Eed	diffuse horizontal irradiance (w/m^2)
Edvm	horizontal sky illuminance calculated from the measured 145 scan points (lux)
Edvp	horizontal sky illuminance calculated from the predicted 145 scan points (lux)
Ees	normal irradiance (w/m^2)
Eeo	extraterrestrial normal irradiance.
L_{cie_cl}	luminance at considered point using CIE standard clear sky (Kcd/m^2)
L_{cie_ct}	luminance at considered point using CIE standard clear-turbid sky (Kcd/m^2)
L_{cie_in}	luminance at considered point using CIE standard intermediate Sky (Kcd/m^2)
L_{cie_ov}	luminance at considered point using CIE standard overcast Sky (Kcd/m^2)
Lmi	measured luminance for scan point i (Kcd/m^2)
Lpi	calculated luminance for scan point i (Kcd/m^2)
Lv	luminance of a sky element (Kcd/m^2).
Lz	zenith luminance (Kcd/m^2)
m	optical mass
N	total number of scan point 145
χ	angle between the sun and the sky point.
Z	angle between the zenith and the sky point.
Zs	angle between the zenith and the sun.
γ	the altitude of sky point.
γs	the altitude of sun.

References

1. Li, D.H.W.; Tsang, E.K.W. An analysis of daylighting performance for office buildings in Hong Kong. *Build. Environ.* **2008**, *43*, 1446–1458. [CrossRef]
2. Alshaibani, K. Potentiality of daylighting in a maritime desert climate: The Eastern coast of Saudi Arabia. *Renew. Energy* **2001**, *23*, 325–331. [CrossRef]
3. Futrell, B.J.; Ozelkan, E.C.; Brentrup, D. Optimizing complex building design for annual daylighting performance and evaluation of optimization algorithms. *Energy Build.* **2015**, *92*, 234–245. [CrossRef]
4. Collins, B.L. Review of the psychological reaction to windows. *Light. Res. Technol.* **1976**, *8*, 80–88. [CrossRef]
5. Boyce, P.; Hunter, C.; Howlett, O. *The Benefits of Daylight through Windows*; Rensselaer Polytechnic Institute: Troy, NY, US, 2003.

6. Altomonte, S. Daylight and the Occupant. Visual and Physio-psychological well-being in built environments. In Proceedings of the Plea2009—26th Conference on Passive and Low Energy Architecture, Quebec, QC, Canada, 22–24 June 2009.
7. Knoop, M. Daylight: What makes the difference? *Light. Res. Technol.* **2020**, *52*, 423–442. [CrossRef]
8. Aries, M.; Aarts, M.; van Hoof, J. Daylight and health: A review of the evidence and consequences for the built environment. *Light. Res. Technol.* **2015**, *47*, 6–27. [CrossRef]
9. Kittler, R.; Perez, R.; Darula, S. A new generation of sky standards. *Proc. Lux Eur. Amst.* **1997**, *1997*, 359–373.
10. Commission International de l'Eclairage. *Spatial Distribution of Daylight—CIE Standard of General Sky, CIE Standard S 011/E: 2003*; February: Viena, Austria, 2003.
11. International Standard Organisation. *Spatial Distribution of Daylight—CIE Standard General Sky*; CIE Central Bureau: Vienna, Austria, 2004.
12. Tregenza, P. Analysing sky luminance scans to obtain frequency distributions of CIE Standard General Skies. *Light. Res. Technol.* **2004**, *36*, 271–281. [CrossRef]
13. Kittler, R.; Darula, S. The simultaneous occurrence and relationship of sunlight and skylight under ISO/CIE standard sky types. *Light. Res. Technol.* **2015**, *47*, 565–580. [CrossRef]
14. Alshaibani, K. Finding frequency distributions of CIE Standard General Skies from sky illuminance or irradiance. *Light. Res. Technol.* **2011**, *43*, 487–495. [CrossRef]
15. Alshaibani, K.A. Classification Standard Skies: The use of horizontal sky illuminance. *Renew. Sustain. Energy Rev.* **2017**, *73*, 387–392. [CrossRef]
16. Li, D.H.W.; Chau, T.C.; Wan, K.K.W. A review of the CIE general sky classification approaches. *Renew. Sustain. Energy Rev.* **2014**, *31*, 563–574. [CrossRef]
17. de Simón-Martín, M.; Alonso-Tristán, C.; Díez-Mediavilla, M. Diffuse solar irradiance estimation on building's façades: Review, classification and benchmarking of 30 models under all sky conditions. *Renew. Sustain. Energy Rev.* **2017**, *77*, 783–802. [CrossRef]
18. Noorian, A.M.; Moradi, I.; Kamali, G.A. Evaluation of 12 models to estimate hourly diffuse irradiation on inclined surfaces. *Renew. Energy* **2008**, *33*, 1406–1412. [CrossRef]
19. Notton, G.; Poggi, P.; Cristofari, C. Predicting hourly solar irradiations on inclined surfaces based on the horizontal measurements: Performances of the association of well-known mathematical models. *Energy Convers. Manag.* **2006**, *47*, 1816–1829. [CrossRef]
20. Li, D.H.W.; Lam, J.C. Evaluation of Perez slope irradiance and illuminance models against measured Hong Kong data. *Int. J. Ambient. Energy* **1999**, *20*, 193–204. [CrossRef]
21. Lam, K.P.; Mahdavi, A.; Ullah, M.B.; Ng, E.; Pal, V. Evaluation of six sky luminance prediction models using measured data from Singapore. *Light. Res. Technol.* **1999**, *31*, 13–17. [CrossRef]
22. Perez, R.; Michalshy, J.; Seals, R. Modeling sky luminance angular distribution for real sky conditions: Experimental evaluation of existing algorithms. *J. Illum. Eng. Soc.* **1992**, *21*, 84–92. [CrossRef]
23. Chaiwiwatworakul, P.; Chirarattananon, S. Evaluation of sky luminance and radiance models using data of north Bangkok. *Leukos* **2005**, *1*, 107–126. [CrossRef]
24. Jones, N.L.; Reinhart, C.F. Effects of real-time simulation feedback on design for visual comfort. *J. Build. Perform. Simul.* **2019**, *12*, 343–361. [CrossRef]
25. Xiong, J.; Tzempelikos, A.; Bilionis, I.; Karava, P. A personalized daylighting control approach to dynamically optimize visual satisfaction and lighting energy use. *Energy Build.* **2019**, *193*, 111–126. [CrossRef]
26. Leccese, F.; Salvadori, G.; Tambellini, G.; Kazanasmaz, Z.T. Application of climate-based daylight simulation to assess lighting conditions of space and artworks in historical buildings: The case study of Cetacean gallery of the monumental charterhouse of Calci. *J. Cult. Herit.* **2020**, in press. [CrossRef]
27. Vera, S.; Uribe, D.; Bustamante, W.; Molina, G. Optimization of a fixed exterior complex fenestration system considering visual comfort and energy performance criteria. *Build. Environ.* **2017**, *113*, 163–174. [CrossRef]
28. Hosseini, S.M.; Mohammadi, M.; Rosemann, A.; Schröder, T. Quantitative investigation through climate-based daylight metrics of visual comfort due to colorful glass and orosi windows in iranian architecture. *J. Daylighting* **2018**, *5*, 21–33. [CrossRef]
29. He, Y.; Zhang, X.; Quan, L. Estimation of hourly average illuminance under clear sky conditions in Chongqing. *PLoS ONE* **2020**, *15*, e0237971. [CrossRef]
30. Costanzo, V.; Evola, G.; Marletta, L.; Nascone, F.P. Application of climate based daylight modelling to the refurbishment of a school building in sicily. *Sustainability* **2018**, *10*, 2653. [CrossRef]

31. Zheng, C.; Wu, P.; Costanzo, V.; Wang, Y.; Yang, X. Establishment and Verification of Solar Radiation Calculation Model of Glass Daylighting Roof in Hot Summer and Warm Winter Zone in China. *Procedia Eng.* **2017**, *205*, 2903–2909. [CrossRef]
32. Lou, S.; Li, D.H.W.; Huang, Y.; Zhou, X.; Xia, D.; Zhao, Y. Change of climate data over 37 years in Hong Kong and the implications on the simulation-based building energy evaluations. *Energy Build.* **2020**, *222*, 110062. [CrossRef]
33. Ineichen, P.; Molineaux, B.; Perez, R. Sky luminance data validation: Comparison of seven models with four data banks. *Sol. Energy* **1994**, *52*, 337–346. [CrossRef]
34. Gracia, A.; Torres, J.L.; de Blas, M.; García, A.; Perez, R. Comparison of four luminance and radiance angular distribution models for radiance estimation. *Sol. Energy* **2011**, *85*, 2202–2216. [CrossRef]
35. Ferraro, V.; Mele, M.; Marinelli, V. Sky luminance measurements and comparisons with calculation models. *J. Atmos. Sol. Phys.* **2011**, *73*, 1780–1789. [CrossRef]
36. Perraudeau, M. Luminance models. In Proceedings of the CIBSE National Lighting Conference, Cambridge, UK, 5–8 April 1988; pp. 291–292.
37. Brunger, A.P.; Hooper, F.C. Anisotropic sky radiance model based on narrow field of view measurements of shortwave radiance. *Sol. Energy* **1993**, *51*, 53–64. [CrossRef]
38. Torres, J.L.; Torres, L.M. Angular distribution of sky diffuse radiance and luminance. In *Modeling Solar Radiation at the Earth's Surface*; Springer: Berlin/Heidelberg, Germany, 2008; pp. 427–448.
39. Harrison, A.W. Directional sky luminance versus cloud cover and solar position. *Sol. Energy* **1991**, *46*, 13–19. [CrossRef]
40. Matsuura, K.; Iwata, T. A model of daylight source for the daylight illuminance calculations on the all weather conditions. In Proceedings of the 3rd International Daylighting Conference, Moscow, Russia, 7–9 February 1990; NIISF: Moscow, Russia, 1990.
41. Commission International de l'Eclairage. *Standardization of the Luminance Distribution on Clear Skies*; CIE: Paris, French, 1973.
42. Moon, P.; Spencer, D.E. Illumination from a non-uniform sky. *Illum. Eng.* **1942**, *37*, 707–726.
43. Matsuura, K. *Luminance Distributions of Various reference Skies*; CIE Technical Report of TC 3-09; International Commission on Illumination: Vienna, Austria, 1987.
44. Perez, R.; Ineichen, P.; Seals, R.; Michalsky, J.; Stewart, R. Modeling daylight availability and irradiance components from direct and global irradiance. *Sol. Energy* **1990**, *44*, 271–289. [CrossRef]
45. Perez, R.; Seals, R.; Michalsky, J. All-weather model for sky luminance distribution—Preliminary configuration and validation. *Sol. Energy* **1993**, *50*, 235–245. [CrossRef]
46. Igawa, N. Improving the All Sky Model for the luminance and radiance distributions of the sky. *Sol. Energy* **2014**, *105*, 354–372. [CrossRef]
47. Ullah, M.B.; Aharari, W. An analysis of climatic variables for thermal design of building in Dhahran. *Arab. J. Sci. Eng.* **1982**, *7*, 101–110.
48. Zell, E.; Gasim, S.; Wilcox, S.; Katamoura, S.; Stoffel, T.; Shibli, H.; Engel-Cox, J.; AlSubie, M. Assessment of solar radiation resources in Saudi Arabia. *Sol. Energy* **2015**, *119*, 422–438. [CrossRef]
49. Tregenza, P.R.; Perez, R.; Michalsky, J.; Seals, R. *Guide to Recommended Practice of Daylight Measurement*; Commission Internationale de l'éclairage: Vienna, Austria, 1994.
50. Alshaibani, K. The use of sky luminance and illuminance to classify the CIE Standard General Skies. *Light. Res. Technol.* **2015**, *47*, 243–247. [CrossRef]
51. Alshaibani, K.A. The use of horizontal sky illuminance to classify the CIE Standard General Skies. *Light. Res. Technol.* **2016**, *48*, 1034–1041. [CrossRef]
52. Illuminating Engineering Society of North America (IESNA). *The IESNA Lighting Handbook: Reference & Application*; Illuminating Engineering Society of North America: New York, NY, USA, 2000.